InAs quantum dots on GaAs$(\bar{2}\bar{5}11)B$: STM and photoluminescence studies

Y. Temko,[1] T. Suzuki,[1] M. C. Xu,[1] K. Pötschke,[2] D. Bimberg,[2] and K. Jacobi[1,*]
[1]*Fritz-Haber-Institut der Max-Planck-Gesellschaft, Faradayweg 4-6, D-14195 Berlin, Germany*
[2]*Technische Universität Berlin, Hardenbergstrasse 36, D-10623 Berlin, Germany*
(Received 18 June 2004; revised manuscript received 15 October 2004; published 27 January 2005)

The GaAs$(\bar{2}\bar{5}11)B$ surface was prepared by molecular beam epitaxy and analyzed *in situ* by scanning tunneling microscopy (STM) and low-energy electron diffraction. Atomically resolved STM images of GaAs$(\bar{2}\bar{5}11)B$ revealed a 1×1 reconstruction, terminated by Ga dimers. The deposition of 1.5 ML of InAs onto GaAs$(\bar{2}\bar{5}11)B$ resulted in the two- to three-dimensional transition with appearance of small InAs quantum dots (QD's) with a very narrow size distribution and a high number density. Low-index $(0\bar{1}\bar{1})$, $(\bar{1}0\bar{1})$, and $(\bar{1}\bar{1}\bar{1})B$ facets, a rounded vicinal $(00\bar{1})$ region for the main part, and a high-index $(\bar{1}\bar{3}5)B$ surface for a flat base determine a shape of the QD's that is totally unsymmetrical. *Ex situ*–performed photoluminescence measurements revealed a peak of the InAs QD's on GaAs$(\bar{2}\bar{5}11)B$ with a similar intensity to the peak from the InAs QD's on the reference GaAs(001) surface, but with a higher emission energy and a smaller linewidth, indicating an ensemble of QD's, smaller and more uniform in size. A small redshift (from 1.33 eV to 1.20 eV) of the emission energy was achieved by optimizing the preparation parameters.

DOI: 10.1103/PhysRevB.71.045336 PACS number(s): 68.65.Hb, 68.37.Ef, 81.05.Ea, 68.35.Bs

I. INTRODUCTION

Self-organized InAs quantum dots (QD's) have been extensively investigated until recently because of their (theoretically predicted) possibility to work as active media in injection lasers operating in the datacom wavelength at 1.3–1.55 μm with some improved properties.[1–3] The QD's of technological interest form due to the Stranski-Krastanow (SK) growth mode, which often occurs in heteroepitaxial systems with significant lattice mismatch (e.g., for InAs/GaAs it is 7.2%). Three-dimensional (3D) InAs islands abruptly arise on the 2D wetting layer (WL) when the amount of deposited material exceeds a critical thickness which is about 1.5–1.8 monolayer (ML) for InAs/GaAs(001). Being composed of a low-band-gap direct semiconductor (e.g., InAs or $In_xGa_{1-x}As$) and embedded in a wide-band-gap substrate (e.g., GaAs), the small-sized QD's confine electrons and holes on discrete atomiclike energy levels and can be employed for getting coherent radiation in the infrared wavelength range.

The main structural properties, affecting the optoelectronic behavior of QD's, are the shape, size, and size distribution. These properties are found to be largely dependent on the orientation and atomic structure of GaAs substrates used. Although the evolution of the InAs QD's is peculiar for each substrate orientation, some common similarities can be extracted analyzing recent publications.[4–15]

(a) The SK transition is realized on all GaAs substrates except for low-index GaAs(110), (111)*A*, and $(\bar{1}\bar{1}\bar{1})B$ surfaces.[4] Note that our definition of the *A* and *B* faces is as follows: A surface in the vicinity of (111)*A* (with threefold-coordinated Ga atoms) is an "*A* face," and a surface in the vicinity of $(\bar{1}\bar{1}\bar{1})B$ (with threefold coordinated As atoms) is a "*B* face." For a graphic illustration see also Ref. 40.

(b) The symmetry of the QD's derives directly from the bulk-truncated substrate that unambiguously proves epitaxial growth during the SK transition.[5–9]

(c) The QD ensemble on a *B* face exhibits a narrower size distribution and a larger number density than that on the respective *A* face.[6–9]

(d) The InAs QD's on the *A* face tend to adopt an elongated shape, whereas those on the *B* face are rather round.[8]

(e) The QD's start to grow with the flattest stable facets with respect to the substrate, which are {2 5 11}*A* or {137}*A* for the GaAs(001) (Ref. 5), GaAs(113)*A* (Ref. 7) and GaAs(2 5 11)*A* (Ref. 11), and $\{\bar{1}\bar{3}5\}B$ (Ref. 15) for the GaAs$(\bar{1}\bar{1}3)B$ (Ref. 6). At the mature stage the islands adopt a steeper shape, terminated by low-index regions.[5–9,12] This final shape seems to remain further unchanged, even by incorporation of dislocations onto the QD's, except for small modifications, like a shape elongation or faceting of the rounded {001} region. Although unstable as nominal GaAs surfaces, large areas of the (137)*A* (Refs. 13 and 14) or $\{\bar{1}\bar{3}5\}B$ (Ref. 16) facets develop on the strained InAs QD's.

All above-considered general QD properties may be verified or even supplemented by employment the two new stable GaAs substrates recently discovered in our group, i.e., GaAs(2 5 11)*A* (Ref. 17) and GaAs$(\bar{2}\bar{5}11)B$. In this contribution we report on the InAs QD's on GaAs$(\bar{2}\bar{5}11)B$. In contrast to the other GaAs substrates, which have already been reported as being stable, the GaAs$(\bar{2}\bar{5}11)B$ surface is an absolute "virgin soil." It has never been mentioned in any paper as being stable or unstable, although the discovery of stable GaAs(2 5 11)*A* presumably implies the stability of GaAs$(\bar{2}\bar{5}11)B$, since among the GaAs surfaces there is no stable *A* face without a stable *B* one so far. Under this premise three questions arise in the following sequence: (a) is GaAs$(\bar{2}\bar{5}11)B$ a stable surface? If so, then (b) does the SK growth mode occur on it? And if so, then (c) what is the optical quality of the resulting QD's? These questions are successively addressed in the present paper by means of the

scanning tunneling microscopy [(STM) *in situ*] and photoluminescence (PL) measurements. Although we have already reported on the atomically resolved shape of the InAs QD's on GaAs($\bar{5}211$)*B*,[9,18] we find it reasonable to integrate the previous results in this paper to make the picture complete and to understand the optical properties of the QD's.

As we have learned from the comparison between InAs QD's on GaAs(113)*A* and *B*, an uniform QD ensemble occurs only on the *B* face.[8] This difference has been attributed to a rough undulating morphology of the bare GaAs(113)*A* surface that became even more corrugated after the InAs deposition up to the SK transition in contrast to the behavior of the GaAs($\bar{1}\bar{1}3$)*B* surface. Except for the formation of step bunches, the GaAs(2 5 11)*A* surface and InAs WL on GaAs(2 5 11)*A* are free of undulations.[11] Therefore, we expected the GaAs($\bar{2}\bar{5}11$)*B* surface to be a very suitable substrate for QD evolution. Hence we have investigated the atomic structure and the morphology of the bare GaAs($\bar{2}\bar{5}11$)*B* surface and the InAs heteroepitaxy on this substrate.

Our paper is organized as follows: In Sec. II we give some experimental details. In Sec. III we combine results and discussion for the bare GaAs($\bar{2}\bar{5}11$)*B* surface and the structural and optical properties of the InAs QD's grown on this substrate. The conclusion follows in Sec. IV.

II. EXPERIMENT

The experiments were carried out in a multichamber ultrahigh vacuum (UHV) system equipped with molecular beam epitaxy (MBE) and STM chambers (Park Scientific Instruments, VP2).[19] Samples with a size of 5×10 mm^2 were cut from a GaAs($\bar{2}\bar{5}11$)*B* wafer (liquid-encapsulated Czochralski-grown GaAs single crystal, 0.2° off-orientation, Si-doped, carrier concentration 10^{18} cm^{-3}, MaTecK). They were glued on a massive (55 g) Ta holder with liquid In. After oxide desorption at a temperature $T\sim600$ °C, the samples were treated with several ion-bombardment and annealing cycles in UHV. The annealing was carried out under As_2 flux (at an As_2 pressure of 4.6×10^{-7} mbar) at 530–580 °C. The temperature was measured by a pyrometer that was calibrated against the GaAs(001)-$c(4\times4)$ to $\beta2(2\times4)$ transition at 465 ± 10 °C. Subsequently, GaAs buffer layers 200–2000 Å were grown by MBE at the rates between 0.1 and 1.5 Å/s as was calibrated with reflection high-energy electron diffraction (RHEED) oscillations of the specular spot acquired during epitaxial growth of GaAs on GaAs(001). During annealing and growth, the surface periodicity and quality was monitored by RHEED. An As_2:Ga beam equivalent pressure (BEP) ratio was set to 7–20. Note that the diffraction patterns of fairly good quality from GaAs($\bar{2}\bar{5}11$)*B* appeared only after some GaAs growth. To get the best quality of the bare surface for STM measurements, the samples were kept at the temperature of 550 °C for 5 min without an As_2 supply from the Knudsen cell—i.e., under less As-rich conditions.

The samples were then cooled down to 430–470 °C and InAs was deposited at a growth rate of 0.075 Å/s and an As_2:In BEP ratio of about 70. The growth rate of InAs was calibrated with RHEED oscillations of the specular spot acquired during epitaxial growth of InAs on InAs(001). After deposition of a 4.5 ± 0.4 Å thick layer of InAs [$\equiv$1.5 InAs(001) monolayer] onto GaAs($\bar{2}\bar{5}11$)*B*, sharp spots appeared in the RHEED pattern along [$2\bar{3}1$] indicating QD formation. The sample heater and the In- and As-Knudsen cells were shut off, as soon as the RHEED pattern changed from streaky to spotty. For the reference photoluminescence measurements the GaAs(001) surface (vertical-gradient-freeze-grown GaAs single crystal, 0.1° off-orientation, undoped, Wafer Technology) was prepared under equal conditions as used for GaAs($\bar{2}\bar{5}11$)*B*. The SK transition occurs on GaAs(001) at an InAs deposition of about 1.5 ML, which is slightly below the reported values of 1.6–1.8 ML for similar preparation conditions except for the InAs growth rate.[5,20] However, the RHEED estimation of the SK transition is fairly rough because it is dependent on the sensitivity of the operator eyes. The amount of InAs material deposited on GaAs($\bar{2}\bar{5}11$)*B* before the SK transition is about equal to that on GaAs(001).

For the STM measurements of the bare and InAs covered GaAs($\bar{2}\bar{5}11$)*B* surface, the samples were transferred to the STM chamber within 30 s and without breaking vacuum (*in situ*). STM images were acquired at room temperature at negative sample biases of from −2.5 to −4.0 V (filled states were imaged) and tunneling currents of 0.1–0.5 nA.

The PL measurements were conducted on the GaAs($\bar{2}\bar{5}11$)*B* and GaAs(001) substrates which were identically prepared. The InAs islands were overgrown with 50 nm GaAs. The first 10 nm were grown at the sample temperature of 450 °C, which was raised then to 520 °C in order to improve the quality of the GaAs cap layer. PL measurements were performed in a closed-cycle He cryostat at 10 K using the 514.5-nm line of an Ar^+ laser for excitation. Excitation densities were set between 5 W/cm^2 (less than one exciton per QD) and 5000 W/cm^2 (more than one exciton per QD). PL was spectrally dispersed by a 0.3-m monochromator and

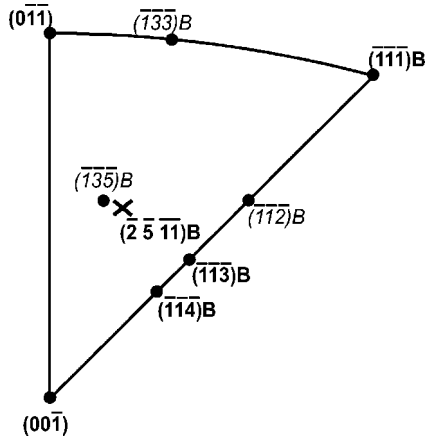

FIG. 1. Stereographic triangle for the GaAs *B* surfaces. The position of the GaAs($\bar{2}\bar{5}11$)*B* is marked with a cross.

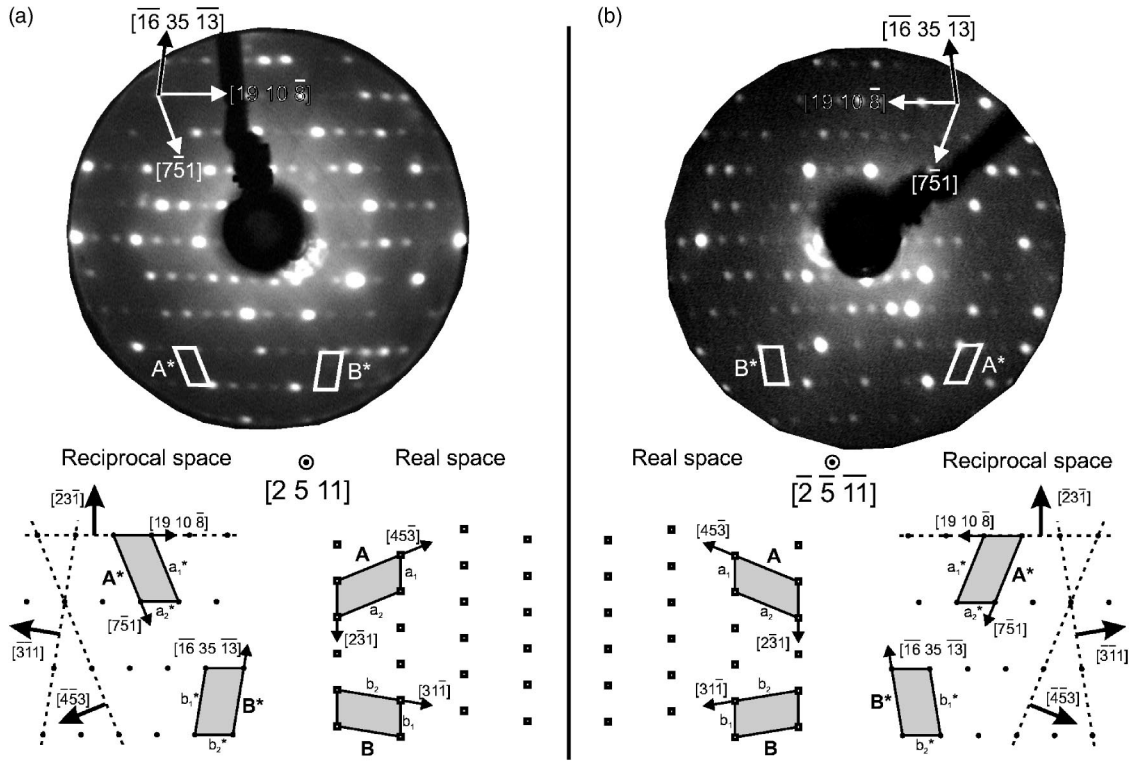

FIG. 2. (a) LEED image of the GaAs(2 5 11)*A* surface ($E=59$ eV) with a schematic sketch of the surface net in reciprocal space (left-hand side) and in real space (right-hand side); (b) LEED image of the GaAs($\overline{2511}$)*B* surface ($E=56$ eV) with a schematic sketch of the surface net in real space (left-hand side) and in reciprocal space (right-hand side). The vertical line between figures (a) and (b) indicates a plane running perpendicular to the GaAs(2 5 11)*A* or *B*, around which the mirror operation has been carried out.

detected with a liquid-N_2-cooled Ge pin diode using lock-in techniques. Note that the STM measurements require highly doped GaAs substrates, whereas for the PL measurements one usually uses semi-insulating GaAs in order to reduce the background signal from the doping levels. Since for the STM technique one needs highly doped substrates, the PL spectra of the GaAs($\overline{2511}$)*B* samples show high background intensity.

III. RESULTS AND DISCUSSION

A. Surface and step structure of the bare GaAs($\overline{2511}$)*B* surface

For the graphic representation of the GaAs($\overline{2511}$)*B* location in space one can use the stereographic projection of the orientations constructed for the *B* faces; i.e., the faces are projected onto the equatorial plane from a point at the north pole of the sphere. Because of the crystallographic symmetry, it is sufficient to restrict these projections to the stereographic triangle (ST) with the (001), (0$\overline{1}$1), and ($\overline{1}$11)*B* low-index surfaces at its corners. The GaAs($\overline{2511}$)*B* surface is situated within the ST and is surrounded by some *B* faces, mentioned in the literature, as shown in Fig. 1.

Stable GaAs *B* surfaces have been found only on the ST edges: the ($\overline{1}$11)*B*,[21] {$\overline{1}$13}*B*,[22] and {$\overline{1}$14}*B*.[23] The structure of the GaAs($\overline{1}$11)*B*-(2×2) As trimer[24] and GaAs($\overline{1}$13)*B*-(1×1) As-rich surfaces[25] has been calculated using density-functional theory. The GaAs($\overline{1}$12)*B* (Refs. 25 and 26) and GaAs{$\overline{1}$33}*B* (Ref. 27) on the ST edges and GaAs{$\overline{1}$35}*B* (Ref. 16) inside the ST are found to decompose into stable GaAs surfaces. We will show that up to now GaAs($\overline{2511}$)*B* is the only known stable *B* surface located within the ST.

In order to understand the surface structure of GaAs($\overline{2511}$)*B* it is convenient to refer to the surface structure of GaAs(2 5 11)*A*. Low-energy electron diffraction (LEED) images of GaAs(2 5 11)*A* and *B* are compared in Figs. 2(a) and 2(b), respectively. A simple mirroring of a 2D net in reciprocal space on the LEED image in Fig. 2(a) leads to a complete superposition of the LEED spots in reciprocal space in Fig. 2(b) [in Fig. 2 this mirroring is carried out around the (19 10 $\bar{8}$) plane]. Note that the intensities of the LEED spots differ after the mirroring, indicating a different atomic filling of the unit cell as expected. The same operation transfers the real space unit cells into each other as shown in Figs. 2(a) and 2(b) below the respective LEED images.

The spots on the LEED image in Fig. 2(b) are very sharp, which indicates a high surface perfection. Almost all reflexes are visible which is different from other stable high-index surfaces.[22,28] A splitting of spots (indicating faceting) in the LEED image in Fig. 2(b) is not observed, which is the first evidence for the stability of the GaAs($\overline{2511}$)*B* surface. Since the spots in (a) are arranged in an oblique net with two dif-

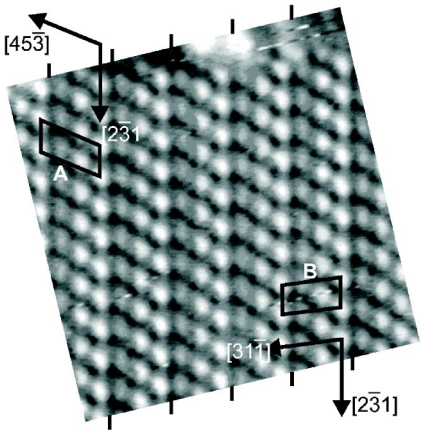

FIG. 3. High-resolution STM image of the GaAs($\overline{2511}$)*B* surface. The solid markers at the image border indicate the trenches between the dimer stripes. The unit meshes *A* and *B* are depicted as black parallelograms. (120×120) Å^2, $U=-2.55$ V, and $I=0.1$ nA.

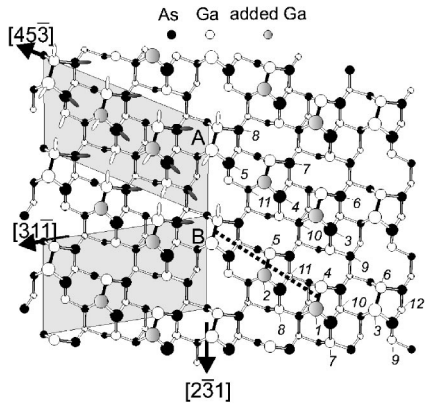

FIG. 4. Top view of a ball-and-stick model for the 1×1 reconstructed GaAs($\overline{2511}$)*B* surface. The size of the circles representing the atoms was chosen according to their vertical distance from the uppermost atom. To arrive at the reconstructed surface, the lighter shaded Ga atoms have been added to the bulk-truncated surface. The numbers near the As and Ga atoms show which atomic layer they belong to, counting from the top. Within unit mesh *A* DB's are included, the As atoms are depicted with black (solid) DB's, the Ga atoms with white (open) DB's.

ferent smallest unit cells, two different unit cells A^* and B^* can also be extracted from the periodicity in (b). As the areas of both unit cells are equal, they both are equivalent. Note that none of the real-space basis vectors in Figs. 2(a) and 2(b) are parallel to any of the reciprocal-space basis vectors because of the oblique surface unit cells. The extracted lengths of the ($\overline{2511}$)*B* basis vectors for unit cells A^* and B^* from LEED images are in real space equal to (11.0±0.5) Å and (20.0±0.5) Å, with an enclosed angle of (67±2)° and (11.0±0.5) Å and (18.5±0.5) Å, with an enclosed angle of (80±2)°, respectively. Hence, there is a large similarity for the structure of the GaAs(2 5 11)*A* and *B* surfaces.

A high-resolution (120×120) Å^2 STM image of the GaAs($\overline{2511}$)*B* surface is shown in Fig. 3. The surface consists of stripes along [2$\bar{3}$1] marked by solid lines on the image border. The stripes contain a little series of three white humps. These series in neighboring stripes are phase shifted; i.e., they are not aligned, but each series in the next stripe is located between the series in the previous stripe. As can be seen, lines of deep holes separate the stripes.

Two shortest unit meshes labeled *A* and *B* can be constructed from the periodicity in Fig. 3. As has been shown in Ref. 29, it is convenient for the structural model to use the unit mesh *A* (comprising a complete series of As dimers) together with the unit mesh *B* (exhibiting the shortest unit vectors). They correspond to the unit cells A^* and B^* in reciprocal space on the LEED image in Fig. 2(b). The lengths of the vectors measured from the STM images are in perfect agreement with those from a model (see below). For unit mesh *A* the lengths are 10.6 and 20.0 Å, and the enclosed angle is 67.8°; the respective values for mesh *B* are 10.6 Å, 18.9 Å, and 80.7°. The vectors of mesh *A* are directed along [45$\bar{3}$] and [2$\bar{3}$1], those of mesh *B* along [31$\bar{1}$] and [2$\bar{3}$1].

A ball-and-stick model for the GaAs($\overline{2511}$)*B* surface is presented in Fig. 4. In order to get a coincidence of this model with the one for GaAs(2 5 11)*A* one should mirror the latter around any plane perpendicular to (2 5 11), rotate the result by 180° around an axis perpendicular to the surface, and then exchange the As and Ga atoms. These operations are necessary because bulk GaAs does not exhibit inversion symmetry. In contrast to GaAs(2 5 11)*A* (see Ref. 17) the *ab initio* total energy electronic structure calculation has not been performed for the *B* face, and precise positions of the As and Ga atoms are unknown. Therefore, Fig. 4 shows the atomic structure derived from the STM images provided the relaxation of the atoms is similar to that shown in Ref. 17 for the *A* face. Black, white, and grey balls depict As, Ga, and adsorbed Ga atoms, respectively. The 1×1 unit meshes *A* and *B* are shown as shaded parallelograms. The vectors of unit mesh *A* lie along [45$\bar{3}$] and [2$\bar{3}$1]. The unit vectors along [31$\bar{1}$] and [2$\bar{3}$1] form the equivalent unit mesh *B*. Both meshes correspond to the bulk-truncated GaAs($\overline{2511}$)*B* surface onto which two Ga atoms were adsorbed that are depicted as grey balls. This model is in agreement with the experimental fact that the surface becomes well ordered only after some GaAs growth and annealing without supply of As_2. Black bars indicate the Ga—Ga bonds in the Ga dimers. The Ga dimers repose on four As atoms, the two uppermost of which exhibit one dangling bond (DB) per atom. According to the electron-counting rule (ECR), each As DB should be filled with two electrons as well as each Ga—Ga bond of the Ga dimer. Therefore, we assume that on the filled-states STM image in Fig. 3 the Ga dimers together with the underneath lying As DB's make up white humps that are very difficult to resolve into the separated DB's because of the small spacing between these features. The lines of deep holes on the STM image in Fig. 3 may stem from the low-lying Ga dimers whose Ga atoms are numbered 3 and 6 in Fig. 4. The Ga dimers are arranged in the series along [12$\bar{1}$] (see the dotted line in Fig. 4), which is inclined to the surface plane such, that the right-hand side lies higher than the left-hand side. The three Ga dimers form the above-mentioned series that are shifted along [2$\bar{3}$1]. Between the

series there are trenches, which comprise filled As DB's (numbered by 9 on the right-hand side of Fig. 4), taking a positive excess charge of +3/4 electrons and giving the stability to the whole structure. The reconstructed 1×1 unit meshes *A* and *B* contain nine Ga DB's (+27/4 electrons), seven As DB's (−21/4 electrons), and three Ga—Ga bonds (−6/4 electrons), so that the structural model fulfils the ECR and the surface is semiconducting.

Because of the large similarity to GaAs(2 5 11)*A*, we do not show the model for the bulk-truncated (ideal) GaAs($\overline{2}5\overline{1}1$)*B* surface. The main points described in Ref. 29 by the consideration of the bulk-truncated GaAs(2 5 11)*A* surface can also be applied here: Neither the bulk-truncated nor the 1×1 reconstructed GaAs($\overline{2}5\overline{1}1$)*B* surface exhibit any symmetry plane; atoms with two DB's are energetically unfavorable, so the bulk-truncated 1×1 surface does not exist. The Ga dimerization is in accordance with the general principle that the number of DB's at a surface should be as small as possible.

The vertical positions of the atoms, extracted from the bulk-truncated model with an addition of the two adsorbed Ga atoms, are numbered in the right-hand side of Fig. 4 in order to show the complexity of this surface reconstruction. Note that the actual relaxation of the atoms is unknown so far. The spacing between the horizontal atomic planes for GaAs($\overline{2}5\overline{1}1$)*B* is the same as for the *A* face—i.e., only 0.23 Å. The grey Ga atoms occupy the highest positions within the unit meshes. From the third atomic layer on there are one Ga and one As atom in each plane, as the bulk-truncated GaAs($\overline{2}5\overline{1}1$)*B* surface is stoichiometric. The reconstruction comprises nine atomic layers. Beginning from the tenth layer the atoms have bulklike bonds.

The GaAs($\overline{2}5\overline{1}1$)*B* surface morphology is shown in Figs. 5(a) and 5(b). The actual off-orientation extracted from many STM images for GaAs($\overline{2}5\overline{1}1$)*B* seldom exceeded 0.3°. The 1×1 μm^2 large STM image in Fig. 5(a) exhibits many terraces up to 1000 Å in width separated by steps, running roughly along the [$2\overline{3}1$] direction. Across the whole image the surface declines from the left-hand to the right-hand side. The average direction of the off-orientation is approximately [$3\overline{1}1$]. The step height has been measured as ~2 Å. Therefore, we think that these steps are equal to the steps along [$2\overline{3}1$], which have been called type "a" and described in Ref. 13 for the vicinal GaAs(2 5 11)*A* surface, although they often run with an opposite off-orientation direction along [$3\overline{1}1$]; see Fig. 5(b). This figure shows another 5000 $\times$5000 Å^2 large area of the surface with two bunch structures running parallel to the [$3\overline{1}1$] direction. The height of the step bunches on GaAs($\overline{2}5\overline{1}1$)*B* has been measured to be up to 10 Å with ($0\overline{1}1$) step walls up to 30 Å in width. The step bunches occur rather seldom. Except for the smaller angle of the off orientation, the morphology of nominal GaAs($\overline{2}5\overline{1}1$)*B* and (2 5 11)*A* (Ref. 13) surfaces is very similar.

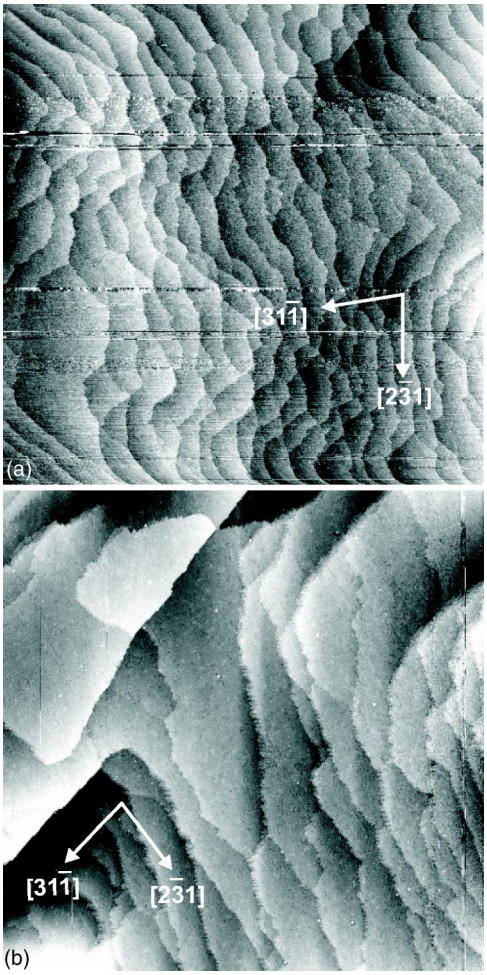

FIG. 5. Overview STM images from two different locations on the nominal GaAs($\overline{2}5\overline{1}1$)*B* surface: (a) ($1\times1$) μm^2, $U=-3.0$ V, $I=0.136$ nA, the off orientation is derived to 0.25° and (b) 5000 $\times$5000 Å^2, $U=-2.5$ V, $I=0.11$ nA, the off orientation is derived to 0.25°.

B. Structural properties of InAs QD's on GaAs($\overline{2}5\overline{1}1$)*B*

An ensemble of InAs QD's on GaAs($\overline{2}5\overline{1}1$)*B* is presented in Fig. 6(a). Many small QD's with an average number density of 1.6×10^{11} cm^{-2} are recognized together with few large islands, one of them being marked by an arrow. All islands develop with the same orientation relative to the substrate and exhibit a uniform shape, which does not change for substrate temperatures during preparation between 430 and 470 °C. The uniformity of the QD ensemble is reflected in the size distribution diagram in Fig. 6(b). About 70% of the islands exhibit a length along [$3\overline{1}1$] between 15 and 20 nm and about 20% of them a length between 10 and 15 nm. (The length is measured at the bottom of the QD along the middle.) The average height of the QD's is 2.2 ± 0.3 nm. This narrow size distribution presumably derives from the elastic strain in the QD's and indicates a coherent (dislocation-free) nature of them. The few large islands contribute to the tail at larger sizes in Fig. 6(b). The large islands do not exhibit a certain size and are probably

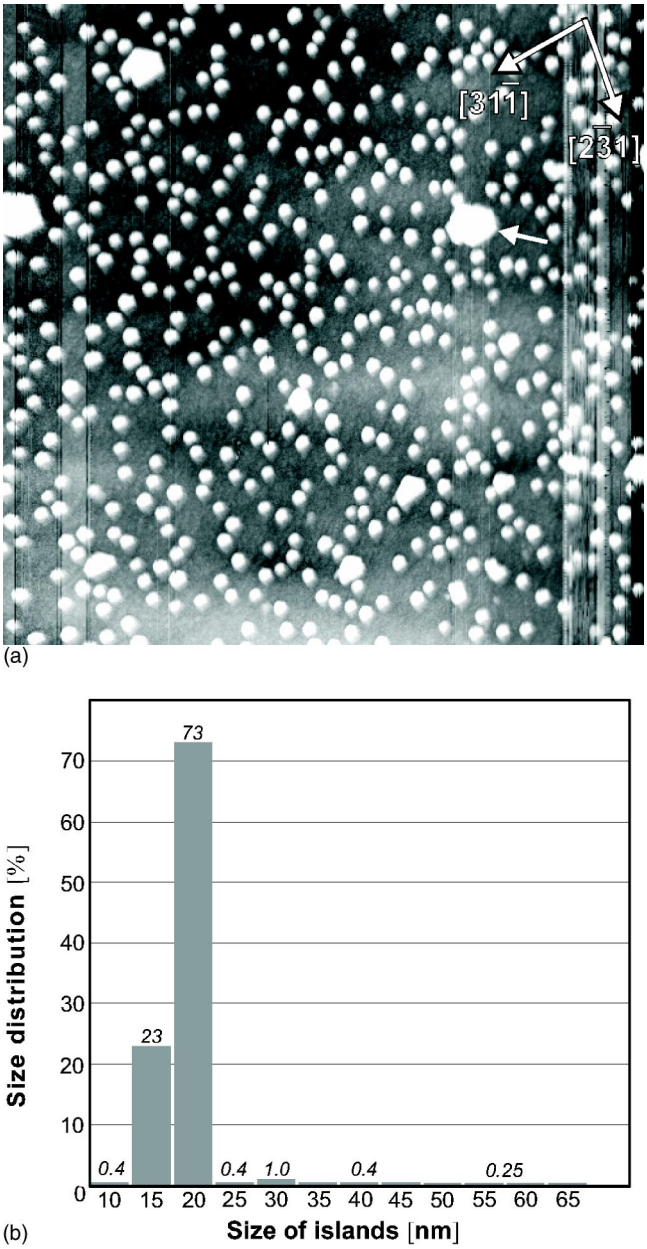

FIG. 6. (a) Overview STM image with InAs QD's grown on GaAs$(\overline{2}511)B$. The white arrow indicates a large incoherent island [(5000×5000) Å^2, $U=-3.5$ V, $I=0.4$ nA, the sample temperature $T=430$ °C, InAs thickness is 4.5 ± 0.4 Å(1.5 ML)]. (b) Size distribution derived from 1560 islands in percent (the % values are given above the respective columns).

formed through coalescence of QD's. They are presumably incoherent; i.e., a dislocation is inserted at the interface.

Figure 7(a) presents a 1000×1000 Å^2 large area of the $(\overline{2}511)B$ surface with InAs QD's. The WL is highly disordered and covered probably with As atoms (because of the As-rich preparation conditions) without any periodicity. That is quite different from the InAs WL on GaAs(2 5 11)*A*,[11] where the original stripes made up from As dimers are still aligned along $[2\overline{3}1]$. On the disordered structure one may expect a great number of broken As bonds, which may catch

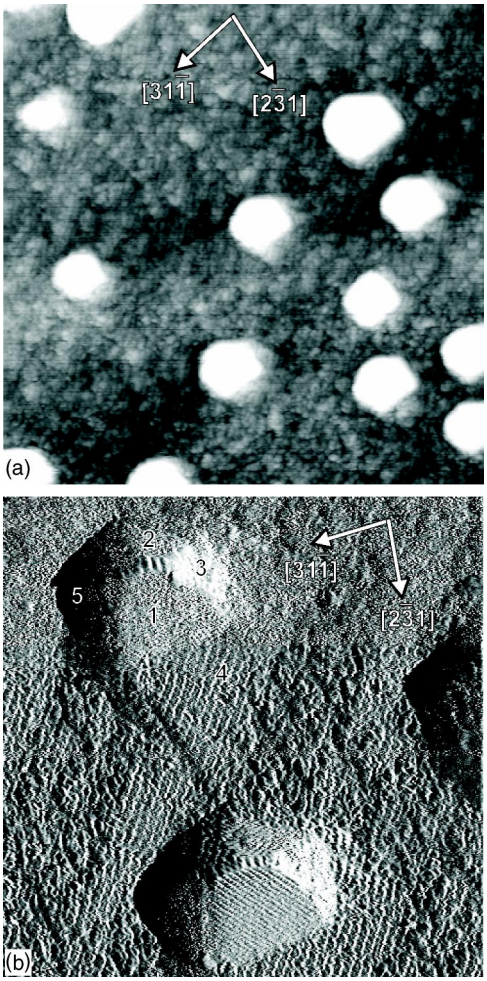

FIG. 7. (a) STM image with InAs QD's grown on a $(\overline{2}511)B$ wetting layer ($U=-3.0$ V, $I=0.1$ nA, $T=430$ °C, 1.5 ML). (b) Atomically resolved STM image (error signal≡constant height mode) of InAs QD's on GaAs$(\overline{2}511)B$ ($U=-3.0$ V, $I=0.3$ nA, $T=450$ °C).

up the cations to form bulklike bonds and, therefore, may slow down their diffusion. This may lead to an increase of the number of nucleation events on the surface and to an increase of the QD number density that is usually higher by one order of magnitude on $(\overline{1}13)B$ (Ref. 6) or $(\overline{2}511)B$ than on $(113)A$ (Ref. 7) or $(2\ 5\ 11)A$ (Ref. 11) substrates. The general problem of As_2 dissociation on the *B* faces and possible difficulties with the incorporation of As_2 on the QD facets—during the evolution of the QD's (Ref. 8)—may yield the effect that the dense array of the QD's grows relatively slowly and In atoms have enough time to check up many islands before an incorporation event. As the smaller islands are believed to grow faster,[30] this would result in a homogeneous, uniform QD ensemble. Thus, the *B* substrates should be generally preferred for the QD application.

Figure 7(b) shows a 600×600 Å^2 large, atomically resolved STM image highlighting the QD shape. The QD's are terminated by several well-developed facets 1–4 and a partially rounded region 5. Facet 4 is a flat base extending in front of facets 1 and 3 on the upper left-hand side of the

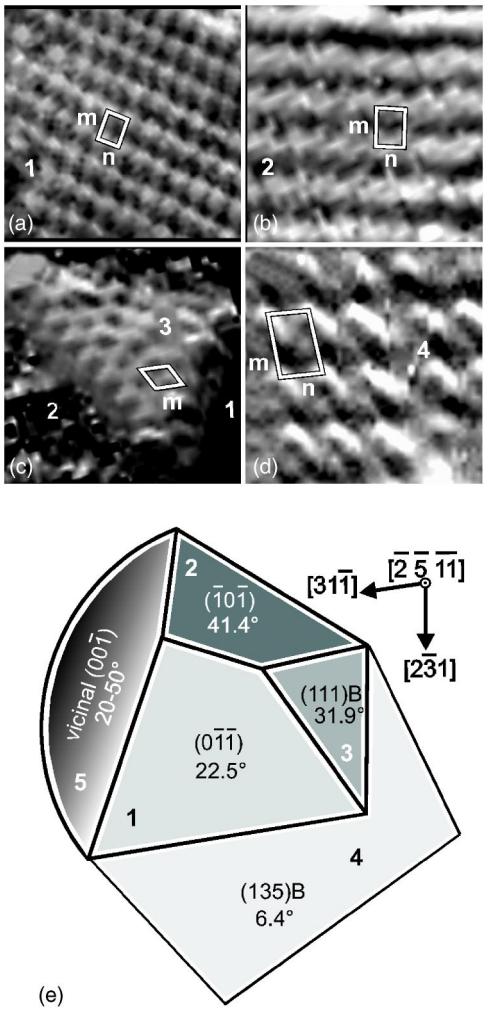

FIG. 8. Atomically resolved STM images (error signal ≡constant height mode, $U=-3.0$ V, $I=0.1$ nA) of (a) the $(01\overline{1})$ facet [the size is (47×47) Å^2], (b) the $(\overline{1}0\overline{1})$ facet [the size is (34×34) Å^2], and (c) the $(\overline{111})B$-(2×2) facet [the size is (78×78) Å^2], and (d) the $(\overline{135})B$-$c(2\times2)$ facet [the size is (48×48) Å^2]. Letters *m* and *n* mark unit cell vectors. (d) Schematic model of InAs QD's on GaAs$(\overline{2511})B$. Darker grey scales correspond to steeper facets.

island in Fig. 7(b). Interestingly, the QD's do not exhibit any symmetry plane perpendicular to the surface. This mirrors the substrate symmetry and is expected for epitaxial growth. Furthermore, similar to the InAs QD's on GaAs$(\overline{113})B$ there is no elongation, in contrast to the respective *A* faces.

In Figs. 8(a)–8(d) we show the individual facets with atomic resolution from which the facet orientation could be derived. Facets 1, 2, 3, and 4 are identified as $(01\overline{1})$, $(\overline{1}0\overline{1})$, $(\overline{111})B$, and $(\overline{135})B$ surfaces, respectively. The comparison between STM data and geometrical values is listed in Table I. The rounded region 5 is not shown in detail in Fig. 8 because it does not exhibit an ordered facet. From geometrical considerations, an $(00\overline{1})$ surface, which is inclined to $(\overline{2511})B$ by 26.1°, should develop in this area. The shape of InAs QD's grown on GaAs$(\overline{2511})B$ is schematically sketched in Fig. 8(e). There is no mirror symmetry on the QD's in agreement with the substrate symmetry. Low-index $(01\overline{1})$, $(\overline{1}0\overline{1})$, and $(\overline{111})B$ facets and a rounded vicinal $(00\overline{1})$ region for the main part, and a high-index $(\overline{135})B$ surface for a flat base, extending in front of the $(01\overline{1})$ and $(\overline{111})B$ facets, determine the shape of the QD's. The facets are inclined to the substrate with different angles, which may result in different growth speed that may be higher for the steeper $(\overline{1}0\overline{1})$ and vicinal $(00\overline{1})$ facets, yielding a compact QD shape without an elongation into any specific direction. In addition, there should be difficulties by the incorporation of As_2 molecules onto all the facets, except for the round region because neither the facets nor the substrate exhibit As dimers as a building blocks for their reconstruction (see also Ref. 8). This facet growth kinetics together with the poorly ordered InAs WL can account for the very narrow size distribution and high number density of the InAs QD's on GaAs$(\overline{2511})B$.

C. Optical properties of InAs QD's on GaAs$(\overline{2511})B$

After having a complete structural characterization and some conclusions on the optical activity, it was very important to test the InAs QD ensemble on GaAs$(\overline{2511})B$ by optical measurements for samples prepared at the same conditions and by the same group. Figure 9 shows normalized PL spectra of one single sheet of InAs QD's with low (5 W cm^{-2}, solid line) and high (5000 W cm^{-2}, dotted line) excitation density. The Gaussian-like PL peak which is centered at 1.34 eV is ascribed to the QD's and has a full width at half maximum (FWHM) of ~45 meV for low excitation density. The small blueshift of the QD luminescence at high excitation density (dotted line) can be explained by the formation of antibonding biexcitons[3] that may appear in the small and unsymmetrical QD's like those shown in Figs. 6–8. The peaks are intense and cover the energy range expected for the small-sized InAs QD's.

For the highest excitation density a second peak arises, which might be induced by the WL. This peak is centered at 1.4 eV and has a FWHM of 25 meV, comparable to the recombination in the InAs WL on GaAs(100).[39] Despite the reduced thermal energy of the carriers at 10 K, the very high density of the InAs QD's on GaAs$(\overline{2511})B$ may allow electrons to find the ground-state level in nearby dots, thus suppressing WL recombination for the excitation densities below 5000 W cm^{-2}. No other peaks are found showing that the InAs QD's on GaAs$(\overline{2511})B$ with the measured diameter of 175±25 Å [see Fig. 6(b)] are so small in size that only the ground-state levels are confined.

It is well known that a vertical stacking of InAs QD's can improve the optical properties of QD lasers and can yield an increase of the active volume, a shift of the emission to longer wavelength, and a decrease of the emission linewidth.[31] This improvement is reported to result from the strain field of underlying dot sheets, which can influence the dot formation in the sheet above, as well as from the electronic coupling of all dots, which increases the effective height and, therefore, reduces the effect of QD size

TABLE I. STM-derived and geometrical values from the individual facets observed for InAs QD's on the GaAs$(\overline{2}5\overline{1}\overline{1})B$ substrate.

Facet No.	Facet plane	Angle against $(\overline{2}5\overline{1}\overline{1})B$ (deg)		Length of unit cell vectors (Å)	
		Expt.	Geom.	Expt.	Geom.
1	$(0\overline{1}\overline{1})$	20±4	22.5	5.9±0.3	6.0
				4.3±0.3	4.0
2	$(\overline{1}0\overline{1})$	38±4	41.4	5.8±0.5	5.5
				4.4±1.0	3.7
3	$(\overline{1}\overline{1}\overline{1})B$	31±3	31.9	8.5±0.8	8.0
				8.5±0.8	8.4
4	$(\overline{1}\overline{3}\overline{5})B$	6±3	6.4	11.3±0.5	11.2
				9.0±0.5	9.6

fluctuations.[32] (A prerequisite is a thin GaAs spacer thickness between the InAs QD sheets up to ten QD heights.) Figure 10 shows the PL spectra of five InAs QD sheets on GaAs$(\overline{2}5\overline{1}\overline{1})B$ with a GaAs spacer thickness of 50 Å, which is roughly twice as large as the average QD height (22–25 Å). The spectra are similar to those in Fig. 9 with exception of the following differences: The intensities of the QD peak (for the same excitation densities) are higher for the vertical stacking; the QD peak is centered at 1.3 eV and shows a FWHM of ~30 meV. Thus, the desirable shift of the emission energy (~34 meV) and a decrease of the linewidth of ~15 meV can clearly be detected for the vertically stacked InAs QD's on GaAs$(\overline{2}5\overline{1}\overline{1})B$. In contrast to the single-QD layer, the stacked QD's show an excited-state transition for highest excitation density with a FWHM of 55 meV as shown in Fig. 10(b). This can be explained by the larger confinement of the stacked dots that also leads to the observed red shift of luminescence. Due to the existence of the excited state (which increases the possible number of excitons per QD from 2 to 6) and the stacking, the probability that the WL is populated is very small. Therefore, the WL luminescence cannot be seen in the PL spectra in Fig. 10 for the 5×QD stacking or, respectively, is overlapped by luminescence from the excited state.

Figure 11 shows a quantitative comparison of the PL spectra of InAs QD's on GaAs$(\overline{2}5\overline{1}\overline{1})B$ and GaAs(001) sub-

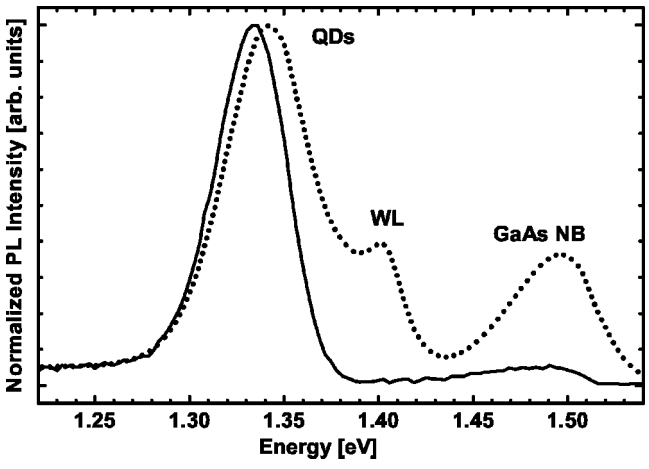

FIG. 9. Normalized linear scale PL spectra of InAs QD's grown on GaAs$(\overline{2}5\overline{1}\overline{1})B$ (T=430 °C, 1.5 ML) acquired with different excitation densities. Excitation density was 5 and 5000 W/cm^2 for solid and dotted lines, respectively. Peaks related to the QD's, the WL, and the GaAs near-band-edge emission are marked.

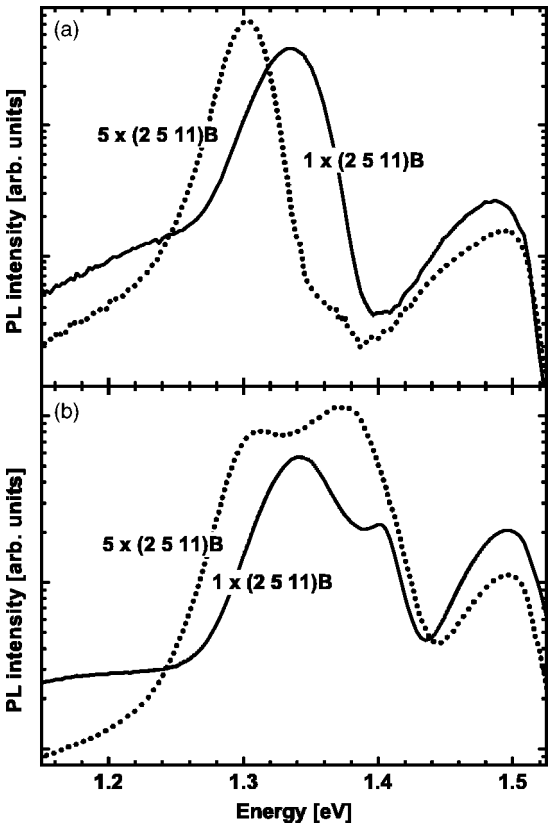

FIG. 10. Decimal logarithmic scale PL spectra of single InAs QD layer (solid line) and 5×QD stacking (dotted line) grown on GaAs$(\overline{2}5\overline{1}\overline{1})B$ (T=430 °C, 1.5 ML) acquired with low (50 W cm^{-2}) (a) and high (5000 W cm^{-2}) (b) excitation density.

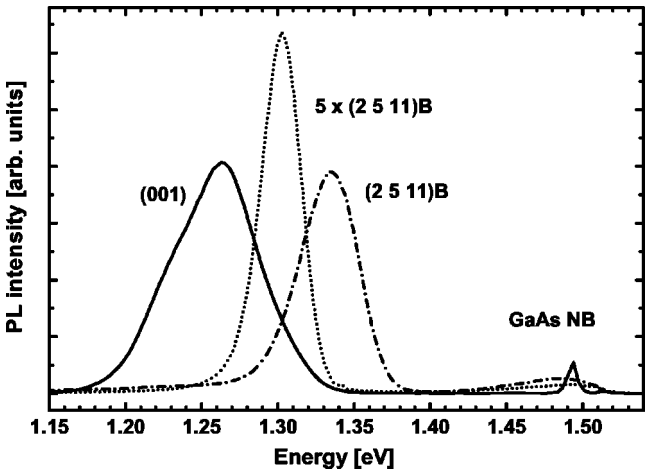

FIG. 11. Linear scale PL spectra of the InAs QDs grown on different GaAs substrates. The QD's and GaAs bulk-related peaks are labeled. Excitation density was 5 W cm^{-2}.

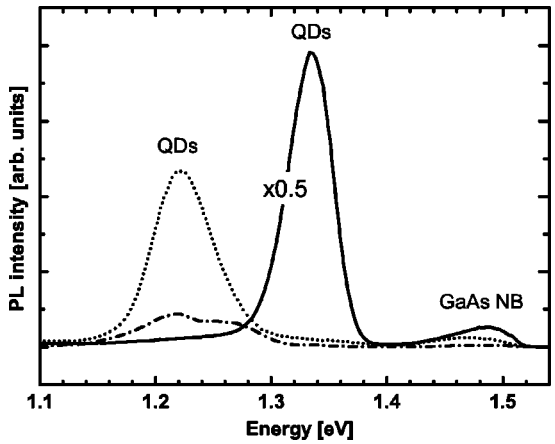

FIG. 12. Linear scale PL spectra of the InAs QD's grown on GaAs($\overline{2511}$)*B* with modified growth conditions. The solid, dotted, and dash-dotted lines correspond to the InAs thickness of 1.5 ML (T=430 °C), 2.0 ML (T=500 °C), and 3.0 ML (500 °C), respectively. The QD's and GaAs bulk-related peaks are labeled. Excitation density was 50 W cm^{-2}.

strates. The solid, dotted, and dash-dotted lines correspond to one single sheet of the QD's on nominal (001), 5× QD stacking on ($\overline{2511}$)*B*, and one single QD sheet on ($\overline{2511}$)*B*, respectively. All QD's are grown at the same sample temperature T=430 °C with an InAs thickness of 1.5 ML to achieve the onset of the SK transition. As can be seen, the Gaussian-like PL peaks of the InAs QD's on GaAs($\overline{2511}$)*B* (dotted and dash-dotted lines) exhibit the same or even higher intensity than the peak of the QD's on commonly used GaAs(001). The PL peaks, depicted by the solid, dotted, and dash-dotted lines, are centered at 1.27, 1.30, and 1.33 eV, with the FWHM values of 66, 30, and 45 meV, respectively. It means that the QD's on GaAs($\overline{2511}$)*B*, prepared under the same MBE conditions, are smaller and more uniform in size than those on GaAs(001). This should be related to the atomic structure of both substrates—i.e., to the differences in adsorption, desorption, and migration of In atoms and As_2 molecules on the differently reconstructed surfaces. The integrated intensity is highest for the GaAs(001) substrate. However, highly doped GaAs($\overline{2511}$)*B* wafers have been used for the PL, which likely results in an absorption of photons by the substrate dopants. Thus, low-doped GaAs($\overline{2511}$)*B* is expected to be suited as a substrate for the growth of InAs QD's with an especially narrow size distribution—i.e., a small PL linewidth.

There is an interest in developing InAs-QD-based devices emitting in the datacom wavelength region around 1.3 μm (954 meV). This would allow the realization of datacom sources cheaper and less temperature sensitive than commonly used InP-based devices.[3] To extend the emission wavelength to 1.3 μm from the single-QD sheet one employs usually some special tricks, among which the first one is to embed the InAs QD's into an $In_xGa_{1-x}As$ matrix (with In content $x<0.3$). A resulting redshift has been observed even beyond 1.3 μm and has been attributed to an increase of the dot height caused by spinoidal-activated decomposition and to a reduced strain in the InAs QD's.[33,34] Another way is to deposit more InAs as needed for the SK transition.[35] The third way is to make large dots by reducing InAs growth rate.[36] However, we use one of the smallest rates reported in the literature (0.075 Å/s=0.025 ML/s, about 60 s to achieve the SK transition). As we have seen for the InAs QD's on GaAs($\overline{113}$)*B* (Ref. 37) an increase of the sample temperature from 435 to 490 °C results in a doubling of the QD size, accompanied, however, by a decrease of QD number density by an order of magnitude. Being unable to perform a systematic PL study because of the lacking of a PL facility at the Fritz-Haber-Institute, we have tried to simultaneously employ all these tricks to shift the emission energy of InAs QD's on GaAs($\overline{2511}$)*B* to the low-energy range.

Figure 12 shows the PL spectra of one single sheet of InAs QD's on GaAs($\overline{2511}$)*B*. The solid line corresponds to a reference sample (Fig. 9) due to the QD's grown at 430 °C with an InAs thickness l=4.5 Å (=1.5 ML_{001}) and overgrown with 50 nm pure GaAs as described in Sec. II. The dotted line stems from the InAs QD's grown at T=500 °C with l=6 Å (=2.0 ML) and overgrown at the same temperature with 7 nm of $In_{0.1}Ga_{0.9}As$ and then with 43 nm of pure GaAs. The solid, dotted, and dash-dotted lines are centered at 1.33 eV (FWHM=44 meV), 1.22 eV (FWHM=62 meV), and 1.22 eV (FWHM=105 meV), respectively. Thus, a redshift can be achieved, however by only 0.1 eV to the value of 1.22 eV, which is of course still far away from 0.95 eV (1.3 μm) needed for the QD applications. The redshift seen for the dotted line is accompanied by a reduction of the integrated PL intensity (by a factor of 4), which is in agreement with our STM observations for InAs QD's on GaAs($\overline{113}$)*B*, where an increased sample temperature yields a decrease of the QD number density.[37] The increase of the FWHM value for the dotted line (in comparison with the solid one) does not agree with the literature (see, e.g., Ref. 38), where a reduced linewidth has been reported for an increase of the sample temperature. The dash-dotted line cor-

responding to the 3-ML InAs QD's, shows a degradation of the single Gaussian-like peak and a high FWHM value. The peak is centred at 1.22 eV, which is next to the PL from 2-ML InAs QD's. It indicates that between 2 and 3 ML of InAs deposition the islands have not increased in size, but have become degraded probably through the incorporation of dislocations after a certain QD size.

As we have shown, it is in principle possible to shift the PL peak of the InAs QD's on GaAs$(\overline{2}511)B$ to smaller energies. One should probably not use the high sample temperature for the overgrowth procedure, which may reduce the QD size through an intermixing of InAs in the GaAs matrix, in order to shift the QD peak further.

IV. CONCLUSION

We prepared here GaAs$(\overline{2}511)B$ and found that it is the only known stable compound semiconductor surface located within the stereographic triangle for the *B* faces. The STM images and LEED pattern indicated a very stable surface structure with a 1×1 reconstruction. The ball-and-stick model of GaAs$(\overline{2}511)B$ is proposed in analogy with that for the *A* face: The mirroring of the GaAs(2 5 11)*A* surface, terminated by As dimers, around any perpendicular plane, and exchanging the As and Ga atoms leads to the GaAs$(\overline{2}511)B$ surface, terminated by Ga dimers. The GaAs$(\overline{2}511)B-1\times1$ reconstruction fulfills the electron counting rule and yields a reduced number of dangling bonds compared with the bulk-truncated surface. No symmetry plane exists on bulk-truncated and reconstructed GaAs$(\overline{2}511)B$. The morphology of the nominal GaAs$(\overline{2}511)B$ surface under investigation exhibited a low off-orientation angle of $\sim0.3°$ and consisted of ~2-Å high steps running mainly along $[2\overline{3}1]$ with a small number of step bunch structures along $[31\overline{1}]$.

The deposition of 1.5 ML of InAs resulted in the SK transition. STM images revealed a uniform ensemble of small InAs QD's on GaAs$(\overline{2}511)B$ with a very narrow size distribution and a high number density. There is no mirror symmetry on the QD's in agreement with the substrate symmetry. Low-index $(0\overline{1}1)$, $(\overline{1}0\overline{1})$, and $(\overline{1}\overline{1}1)B$ facets and a rounded vicinal (001) region for the main part, and a high-index $(\overline{1}35)B$ surface for a flat base, extending in front of the $(0\overline{1}1)$ and $(\overline{1}\overline{1}1)B$ facets, determine the shape of the QD's. The facets are inclined to the substrate with different angles, which may result in different growth speed that may be higher for the steeper $(\overline{1}0\overline{1})$ and vicinal $(00\overline{1})$ facets yielding a compact QD shape without an elongation into any specific direction. In addition, there are probably difficulties for the incorporation of As_2 molecules onto all the facets, except for the rounded region. This facet growth kinetics together with the poorly ordered InAs WL, which can reduce the diffusion length of In atoms, may account for the very narrow size distribution and high number density of the InAs QD's on GaAs$(\overline{2}511)B$.

The Gaussian-like PL peak of the InAs QD's on GaAs$(\overline{2}511)B$ exhibited a similar intensity as from the InAs QD's on commonly used GaAs(001), but a higher emission energy (about 1.3 eV). A smaller FWHM (about 40 meV) indicated a smaller and more uniform size of the QD ensemble on GaAs$(\overline{2}511)B$ in agreement with our STM measurements. A small redshift (from 1.33 to 1.2 eV) of the emission energy was achieved by using vertical stacked QD's or by an increase of the sample temperature and InAs thickness of the dots embedded in a $In_{0.1}Ga_{0.9}As$ cap layer.

ACKNOWLEDGMENT

We thank G. Ertl for support and P. Geng for technical assistance. Y.T. is very thankful to L. Geelhaar from Infineon Technologies AG, Munich for fruitful discussions. The work was supported by the Deutsche Forschungsgemeinschaft (Grant No. SFB296, Project A2).

*Corresponding author. FAX: +49-30-8413-5106. Electronic address: jacobi@fhi-berlin.mpg.de

[1] D. Bimberg, M. Grundmann, and N. N. Ledentsov, *Quantum Dot Heterostructures* (Wiley, Chichester, 1999).

[2] *Semiconductor Quantum Dots*, edited by Y. Masumoto and T. Takagahara (Springer, Berlin, 2002).

[3] *Nano-optoelectronics: Concepts, physics and devices*, edited by M. Grundmann (Springer, Berlin, 2002).

[4] D. Leonard, K. Pond, and P. M. Petroff, Phys. Rev. B **50**, 11 687 (1994); M. Henini, S. Sanguinetti, L. Brusaferri, E. Grilli, M. Guzzi, M. D. Upward, P. Moriarty, and P. H. Beton, Microelectron. J. **28**, 933 (1997); S. C. Fortina, S. Sanguinetti, E. Grilli, M. Guzzi, M. Henini, A. Polimeni, and L. Eaves, J. Cryst. Growth **187**, 126 (1998); J. G. Belk, J. L. Sudijono, X. M. Zhang, J. H. Neave, T. S. Jones, and B. A. Joyce, Phys. Rev. Lett. **78**, 475 (1997); H. Yamaguchi, M. R. Fahy, and B. A. Joyce, Appl. Phys. Lett. **69**, 776 (1996); S. E. Hooper, D. I. Westwood, D. A. Woolf, S. S. Heghoyan, and R. H. Williams, Semicond. Sci. Technol. **8**, 1069 (1993).

[5] J. Márquez, L. Geelhaar, and K. Jacobi, Appl. Phys. Lett. **78**, 2309 (2001).

[6] T. Suzuki, Y. Temko, and K. Jacobi, Appl. Phys. Lett. **80**, 4744 (2002).

[7] Y. Temko, T. Suzuki, and K. Jacobi, Appl. Phys. Lett. **82**, 2142 (2003).

[8] Y. Temko, T. Suzuki, P. Kratzer, and K. Jacobi, Phys. Rev. B **68**, 165310 (2003).

[9] Y. Temko, T. Suzuki, M. C. Xu, and K. Jacobi, Appl. Phys. Lett. **83**, 3680 (2003).

[10] M. C. Xu, Y. Temko, T. Suzuki, and K. Jacobi, Appl. Phys. Lett. **84**, 2283 (2004).

[11] Y. Temko, T. Suzuki, M. C. Xu, and K. Jacobi (unpublished).

[12] G. Costantini, C. Manzano, R. Songmuang, O. G. Schmidt, and K. Kern, Appl. Phys. Lett. **82**, 3194 (2003).
[13] Y. Temko, L. Geelhaar, T. Suzuki, and K. Jacobi, Surf. Sci. **513**, 328 (2002).
[14] K. Jacobi, L. Geelhaar, and J. Márquez, Appl. Phys. A: Mater. Sci. Process. **75**, 113 (2002).
[15] K. Jacobi, Prog. Surf. Sci. **71**, 185 (2003).
[16] T. Suzuki, Y. Temko, M. C. Xu, and K. Jacobi, Surf. Sci. **548**, 333 (2004).
[17] L. Geelhaar, J. Márquez, P. Kratzer, and K. Jacobi, Phys. Rev. Lett. **86**, 3815 (2001).
[18] In this study we have horizontally mirrored the STM results in order to transfer them to the commonly used atomic geometry of the substrate—i.e., (2 5 11)—known from its inventors (see Ref. 17).
[19] P. Geng, J. Márquez, L. Geelhaar, J. Platen, C. Setzer, and K. Jacobi, Rev. Sci. Instrum. **71**, 504 (2000).
[20] Y. Hasegawa, H. Kiyama, Q. K. Xue, and T. Sakurai, Appl. Phys. Lett. **72**, 2265 (1998).
[21] D. K. Biegelsen, R. D. Bringans, J. E. Northrup, and L.-E. Swartz, Phys. Rev. Lett. **65**, 452 (1990).
[22] J. Márquez, L. Geelhaar, and K. Jacobi, Phys. Rev. B **62**, 9969 (2000).
[23] J. Platen, C. Setzer, W. Ranke, and K. Jacobi, Appl. Surf. Sci. **123/124**, 43 (1998).
[24] N. Moll, A. Kley, E. Pehlke, and M. Scheffler, Phys. Rev. B **54**, 8844 (1996).
[25] J. Platen, A. Kley, C. Setzer, K. Jacobi, P. Ruggerone, and M. Scheffler, J. Appl. Phys. **85**, 3597 (1999).
[26] L. Geelhaar, J. Márquez, K. Jacobi, A. Kley, P. Ruggerone, and M. Scheffler, Microelectron. J. **30**, 393 (1999).
[27] S. Horng, K. Young, and A. Kahn, J. Vac. Sci. Technol. A **7**, 2039 (1989).
[28] L. Geelhaar, J. Márquez, and K. Jacobi, Phys. Rev. B **60**, 15 890 (1999).
[29] L. Geelhaar, Y. Temko, J. Márquez, P. Kratzer, and K. Jacobi, Phys. Rev. B **65**, 155308 (2002).
[30] D. E. Jesson, G. Chen, K. M. Chen, and S. J. Pennycook, Phys. Rev. Lett. **80**, 5156 (1998).
[31] G. S. Solomon, J. A. Trezza, A. F. Marshall, and J. S. Harris, Phys. Rev. Lett. **76**, 952 (1996).
[32] M. O. Lipinski, H. Schuler, O. G. Schmidt, K. Eberl, and N. Y. Jin-Phillipp, Appl. Phys. Lett. **77**, 1789 (2000).
[33] M. V. Maximov, A. F. Tsatsul'nikov, B. V. Volovik, D. A. Bedarev, A. E. Zhukova, A. R. Kovsh, N. A. Maleev, V. M. Ustinov, P. S. Kop'ev, Z. I. Alferov, R. Heitz, N. N. Ledentsov, and D. Bimberg, Physica E (Amsterdam) **7**, 326 (2000).
[34] J. X. Chen, A. Markus, A. Fiore, U. Oesterle, R. P. Stanley, J. F. Carlin, R. Houdré, M. Ilegems, L. Lazzarini, L. Nasi, M. T. Todaro, E. Piscopiello, R. Cingolani, M. Catalano, J. Katcki, and J. Ratajczak, J. Appl. Phys. **91**, 6710 (2002).
[35] A. Passaseo, M. De Vittorio, M. T. Todaro, I. Tarantini, M. De Giorgi, R. Cingolani, A. Fiore, A. Markus, J. X. Chen, C. Paranthoen, U. Oesterle, and M. Ilegems, Appl. Phys. Lett. **82**, 3632 (2003).
[36] P. B. Joyce, T. J. Krzyzewski, G. R. Bell, T. S. Jones, E. C. Le Ru, and R. Murray, Phys. Rev. B **64**, 235317 (2001).
[37] T. Suzuki, Y. Temko, and K. Jacobi, Phys. Rev. B **67**, 045315 (2003).
[38] O. G. Schmidt, S. Kiravittaya, Y. Nakamura, H. Heidemeyer, R. Songmuang, C. Müller, N. Y. Jin-Phillipp, K. Eberl, H. Wawra, S. Christiansen, H. Gräbeldinger, and H. Schweizer, Surf. Sci. **514**, 10 (2002).
[39] R. Heitz, T. R. Ramachandran, A. Kalburge, Q. Xie, I. Mukhametzhanov, P. Chen, and A. Madhukar, Phys. Rev. Lett. **78**, 4071 (1997).
[40] http://w3.rz-berlin.mpg.de/pc/ElecSpec/